Cellular Interactions

DOI: 10.1002/anie.201105573

Gold Nanoclusters and Graphene Nanocomposites for Drug Delivery and Imaging of Cancer Cells**

*Chensu Wang, Jingyuan Li, Christian Amatore, Yu Chen, Hui Jiang, and Xue-Mei Wang**

Gold nanoclusters (GNCs) have attracted wide attention owing to their outstanding surface and physical properties (for example, near-infrared photoluminescence,[1] optical chirality,[2] and ferromagnetism[3]), which has led to a wide range of applications, such as for single-molecule photonics, sensing, and biological labeling.[4] In contrast to organic dyes and quantum dots, GNCs do not contain chemical functions and toxic heavy metals.[4b–d] Their near-infrared range of emission avoids interference from many biological moieties, making GNCs ideal for biological assays and cell imaging so that they may become a powerful alternative to usual fluorescence labels.[5]

On the other hand, two dimensional graphene has attracted considerable interest owing to its long-range π conjugation, yielding extraordinary thermal, mechanical, and electrical properties.[6] To date, the chemistry of graphene that has been reported mainly concerns the chemistry of graphene oxide (GO),[6d] which has chemically reactive oxygen-containing groups, including carboxylic acid groups at the edges of GO and epoxy and hydroxy groups on the basal planes. Because electrical conductivity, a large specific Brunauer–Emmett–Teller surface area, and high fracture strength can be recovered by restoring the π network, one of the most important reactions of GO is its reduction.[7] Previous studies have established that graphene, including GO and its reduced form, reduced graphene oxide (RGO), is biocompatible[8] and is a perfect support for a variety of metal and metal oxide nanoparticles, such as Pt, Au, TiO_2,[9] fluorescent molecules, and drugs with potential biochemical applications.[10] Functionalized graphene sheets are thus prone to act as drug delivery platforms, while their near-infrared thermal properties make them attractive multimodal cancer therapeutic agents. Furthermore, RGO could also allow a facile attachment of many molecular drugs and nanomaterials.[6]

RGO has been frequently modified by noncovalent physisorption of polymers, small aromatic molecules, and metal nanoparticles with higher electron affinity, such as gold, onto their basal planes by π–π stacking, cation–π, or van der Waals interactions.[11] For GNC-RGO nanocomposites, it may not only offer new and efficient entries in the current search for multimodal therapeutic materials that are prone to targeting/detecting and treating specifically altered tissues, but also offer attractive alternatives to existing cancer therapeutic techniques. Herein, we explore the biological properties of newly prepared GNC-RGO nanocomposites. This material could cause inhibition of HepG2 cells at high concentration, but more interestingly for oncotherapy it could carry anticancer agents such as doxorubicin (DOX) inside the cells while leading to some synergy in inducing karyopyknosis. It is observed that GNCs anchored on RGO retain their near-infrared fluorescent property so that Raman spectroscopy could be used to investigate the performance of DOX-loaded GNC-RGO nanocomposites against hepatocarcinoma and provide important mechanistic clues about their interactions with proteins and DNA.

GNCs were prepared in the organic phase following a conventional Brust–Schiffrin procedure[12] and transferred into an aqueous phase. Simple mixing of the dodecanethiol-CTAB-capped GNCs with RGO in aqueous solution followed by separation afforded water-soluble GNC-RGO nanocomposites in excellent yields. TEM analysis (Figure 1a) established that 95% of the water-soluble GNCs ranged between 2–3 nm in diameter with a distribution peak at 2.5 nm. They maintained their size distribution and morphology upon attachment to RGO (Figure 1b). HRTEM (Figure 1b, inset) showed that the GNCs kept their interplanar Au–Au spacing at 0.215 nm after attachment onto RGO.

Though common gold nanoparticle sols exhibit a surface plasmon band (SPB), creating a broad absorption band in the visible region around 520 nm and thus their characteristic deep-red color, the color of GNCs and GNC-RGO was faint, in agreement with the fact that no obvious UV/Vis absorbance could be observed in Figure 1c. It is known that Au nanoparticles less than 3 nm in size do not exhibit the surface plasmon resonance characteristic peak at around 520 nm.[11c,13] This result is in good agreement with our observation (Figure 1c) in which the absorption originating

[*] C. Wang,[+] J. Li,[+] Dr. H. Jiang, Prof. X.-M. Wang
State Key Lab of Bioelectronics (Chien-Shiung Wu Laboratory)
Southeast University, No. 2 Sipailou, Nanjing 210096 (China)
E-mail: xuewang@seu.edu.cn
Prof. C. Amatore
Ecole Normale Supérieure, UMR CNRS-ENS-UPMC 8640 and LIA CNRS XiamENS NanoBioChem Département de Chimie (France)
Prof. Y. Chen
Key Laboratory for Advanced Materials
Institute of Applied Chemistry
East China University of Science and Technology
Shanghai (P.R. China)
[+] These authors contributed equally to this work.

[**] In China, this work was supported by the National Key Basic Research Program (2010CB732404), the National Natural Science Foundation of China (21175020), the Doctoral Fund of the Ministry of Education of China (RFDP20090092110028), the Natural Science Foundation of Jiangsu Province (BK2008149), the Fundamental Research Funds for the Central Universities, the Shanghai Eastern Scholarship, the Visiting Scholar Foundation of Key Laboratory of Biorheological Science and Technology (Chongqing University), and the Ministry of Education. In France, it was supported by the CNRS, the ENS, and the UPMC (UMR 8640 and LIA XiamENS).

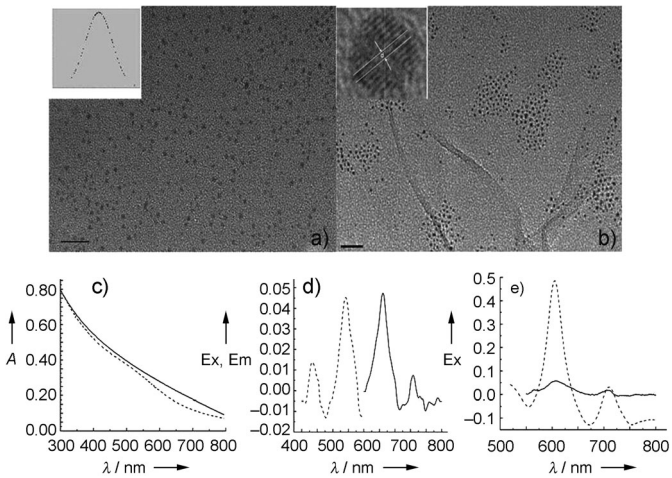

Figure 1. Characterization of GNCs and GNC-RGO. a) TEM image and statistical size distribution (inset; maximum at 2.5 nm) of GNCs. Scale bar: 20 nm. b) TEM image of GNC-RGO, showing the 0.215 nm interplanar spacing of GNCs on RGO (inset). Scale bar: 20 nm. c) UV/Vis spectra of GNCs (-----) and GNC-RGO (——). d) Fluorescent spectra of GNC-RGO in water; the excitation spectrum (Ex, -----) was recorded using a fixed emission at 610 nm while the emission spectrum (Em, ——) was determined upon excitation at 490 nm. e) Fluorescence emission spectra of GNC (-----) and GNC-RGO (——; $\lambda_{Ex} = 490$ nm).

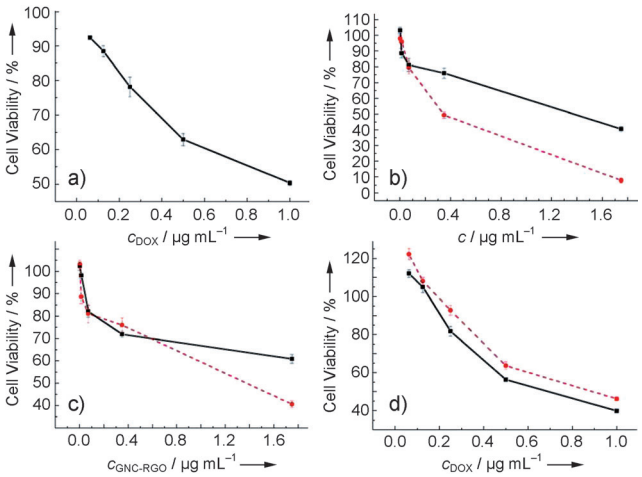

Figure 2. In vitro dose-dependent MTT toxicity tests towards HepG2 cells. a) DOX alone after 24 h incubation. b) GNCs (●, red) and GNC-RGO (■, black) after 48 h incubation. c) Comparison of the cytotoxicity of GNC-RGO after 48 h (●, red) and 72 h incubations (■, black). d) Comparison of the cytotoxicity of DOX-loaded GNC-RGO (■, black) and DOX alone (●, red) to HepG2 cells after 48 h incubation.

from the GNCs was not detected in UV/Vis spectra of relevant nanocomposites (Figure 1c) owing to the small size of GNCs. Figure 1d depicts the fluorescence emission and excitation spectra of GNC-RGO dissolved in water. By using 490 nm excitation light, the steady-state fluorescence spectrum of GNV-RGO displayed two emission peaks at 606 and 705 nm. Lin et al.[4b] reported a (1.83 ± 0.32) % quantum yield for GNCs in water (pH 9), thus placing them in an adequate range for applications in optical devices and biosensors. The fluorescence emission and excitation bands of the present GNC-RGO nanocomposites matched those of GNCs, showing that their fluorescence properties were not noticeably affected by the presence of RGO.

We have tested the relevant drug loading (DL) and encapsulation efficiency (EE). The results indicated that DL could be achieved at 91 % and EE was 40 % when DOX was 0.22 mg mL^{-1} and GNC-RGO was 1 mg mL^{-1}. Figure 2 compares the toxicities (MTT tests) of DOX alone (Figure 2a), GNCs alone, or RGO-GNC composites (Figure 2b and c) to those of DOX-loaded RGO-GNC composites (Figure 2d) towards HepG2 cells. In agreement with the results of Pan et al.[5] GNCs (Figure 2b) cause more serious cytotoxic effects than common gold nanoparticles. GNCs and GNC-RGO have different dose-dependent toxicities above 0.2 μg mL^{-1} (Figure 2b). Fortunately for general applications, GNC-RGO were found to be less toxic than GNCs at the same concentration (Figure 2b; IC50 values: 1.36 μg mL^{-1} for GNC-RGO versus 0.36 μg mL^{-1} for GNCs). GNC-RGO exhibited a marked time-dependent toxicity, though this occurred only above 0.35 μg mL^{-1} (Figure 2c). DOX-loaded GNC-RGO (Figure 2d) inhibited HepG2 cell growth more strongly than DOX and GNC-RGO alone, suggesting that DOX was more effectively transported into the cell cytoplasm by the GNC-RGO platform than when used alone (see below, Figure 4).

Although noncovalent attachment of GNCs onto the RGO surface resulted in a partial fluorescence quenching compared to GNCs, which is presumably due to coulombic electron transfer between GNCs and RGO, both GNCs and GNC-RGO could be readily used for cellular imaging. Figure 3 shows that both are well-distributed within the cells, and that the edge and morphology of the cells are delineated well. Importantly, GNCs were found to cause serious karyopyknosis of HepG2 cells, whereas this happened much less in the cells treated with GNC-RGO, in agreement with their relative dose-dependent abilities to induce necrosis or apoptosis (Figure 2b).

To confirm that GNC-RGO reinforced DOX absorption by HepG2 cells, we relied on the strong spontaneous fluorescence of DOX to follow its distribution in the cells cytoplasm after incubation with or without the presence of GNC-RGO. DOX alone did not distribute well in the cells, with about half of the DOX molecules resting on the cell

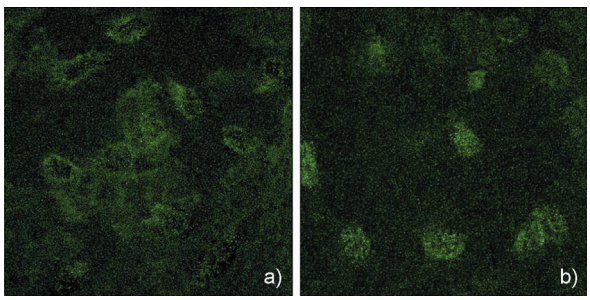

Figure 3. Laser confocal fluorescence micrographs of HepG2 cells treated with a) GNC-RGO 1.75 μg mL^{-1} or b) GNCs 1.75 μg mL^{-1} and incubated for 14 h. Images were acquired at 400-fold magnification.

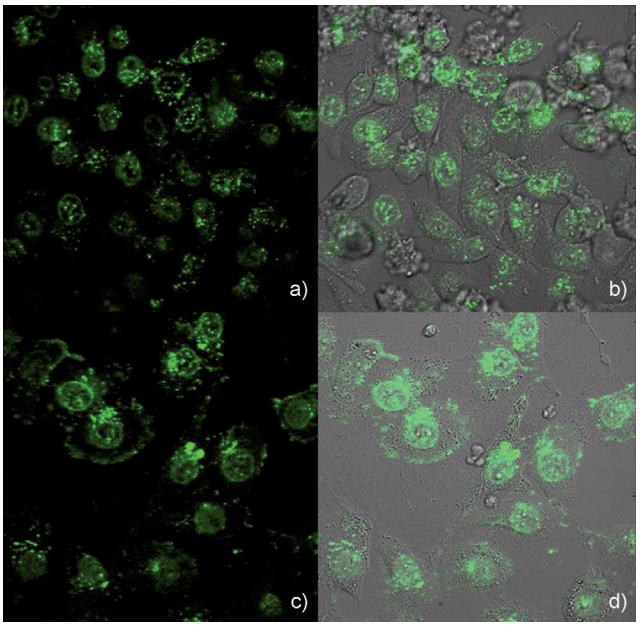

Figure 4. Laser confocal fluorescence micrographs of HepG2 cells treated with 0.25 μg mL^{-1} DOX (a,b) and DOX-loaded GNC-RGO (c,d). a,c) Fluorescence micrographs. b,d) Overlay of the morphological and fluorescence images after incubation for 14 h. Images were acquired at 400-fold magnification.

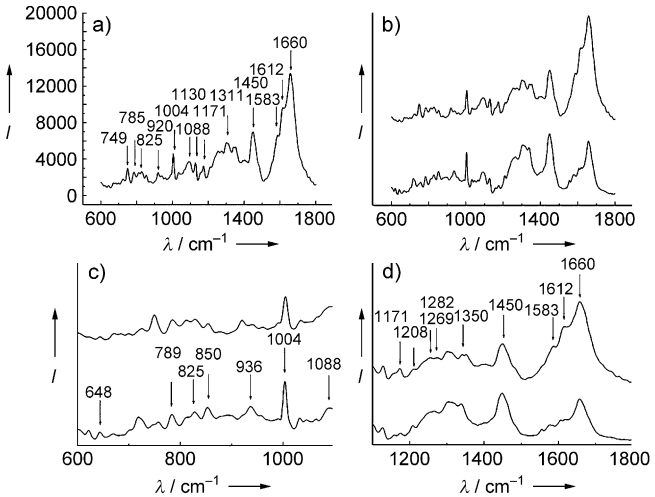

Figure 5. Raman spectra of HepG2 cells before and after incubation with 1.75 μg mL^{-1} GNC-RGO for 24 h. a) Mean Raman spectra of HepG2 cells (control). b) Comparison between the cell spectrum (top) to that of HepG2 cells treated with GNC-RGO (bottom). c) Enlargement of spectra in (b) over the range 600–1100 cm^{-1}; d) Enlargement of spectra in (b) over the range 1100–1800 cm^{-1}. Excitation wavelength: 785 nm.

membrane surface or in between cells (Figure 4a and b). Conversely, when loaded onto GNC-RGO nanocomposites, DOX was well-distributed inside the cells (Figure 4c and d), establishing that GNC-RGO acted as a drug delivery platform that improves DOX internalization by HepG2 cells. This result suggests that GNC-RGO vectorization may have enhanced membrane permeability through interactions with phospholipids and/or proteins, resulting in high drug transfer into the cells.

To further investigate the interaction between GNC-RGO and HepG2 cells, conventional Raman spectra of regular HepG2 cells (Figure 5a) were compared to those of cells treated with GNC-RGO (Figure 5b). Figure 5c and d details the corresponding changes over shorter wavelength windows so as to focus on the interactions between proteins and DNA with GNC-RGO. First, the characteristic band of RGO at about 1350 cm^{-1} [14a] can be seen in the spectrum of cells treated by GNC-RGO (Figure 5d), in agreement with the facile hybrid transfer inside of cells evidenced by the fluorescence data in Figure 4c and d. Surprisingly in view of such facile penetration, there was no noticeable change in the bands relative to the membrane phospholipids indicating the structural conservation of these biomolecules though GNC-RGO swiftly came across the membranes (Figure 3). Such easy transfer may then result from fleeting supramolecular interactions between membrane phospholipids and the nanocomposites lipidic coatings. If so, considering that the nanocomposites residence time in/near the membranes was considerably reduced by the RGO moiety (Figure 3) it seems normal that no drastic change could be observed in the bands characteristic of phospholipids.

Because GNC-RGO nanocomposites were internalized by HepG2 cells (Figure 3) and caused moderate karyopyknosis (Figure 2b), it was of interest to focus on the changes incurred by proteins and DNA. In proteins, the amide III band (1200–1300 cm^{-1}; Figure 5d) is sensitive to the main-chain conformation. Two bands (1269 cm^{-1} and 1282 cm^{-1}),[14] which belong to the α helix, degenerated to a mild band at about 1266 cm^{-1}, while the band at about 1304 cm^{-1},[14b] which belongs to the β folding, was unchanged. This suggests that the presence of GNC-RGO affects the protein α helices but not their β folding. In the conformation of the side chain of protein, tyrosine bands at about 850 and 825 cm^{-1} [14] (Figure 5c) are also conformation sensitive. Upon treatment by GNC-RGO, the relative intensity of these two bands increased by 15.7% (from 0.875 in controls to 1.038), revealing that the environment around the tyrosine side chain was affected. This was supported by the simultaneous increase in intensity of the band at about 1612 cm^{-1},[14c] confirming that GNC-RGO modified the external environment of tyrosine and phenylalanine presumably by exposing part of the tyrosine. In nontreated cancer cells, proteins have an orderly folding structure with the tyrosine and phenylalanine side chain lying in a buried state, thus resulting in a weak Raman scattered signal. Therefore, the above series of changes strongly suggest that in the presence of GNC-RGO nanocomposites, hydrogen bonds were significantly disturbed so as to enforce exposition of the tyrosine and phenylalanine side chain, thereby enhancing the relevant scattered Raman signal intensities.

Concerning DNA, the band at about 785 cm^{-1}, which reflects the symmetric telescopic vibration of PO_2 (BNPP), shifted to 790 cm^{-1} [14a] and increased in its intensity (Figure 5c), showing that GNC-RGO induces DNA disorder. The fact that DNA was affected in the presence of nanocompo-

sites was confirmed by the shift of the band at about 1094 cm^{-1} (which is also reflected in the symmetric telescopic vibration of PO_2) to 1088 cm^{-1}, accompanied by a decrease in intensity (Figure 5c). This points to a rupture of DNA chains. Finally, the intensity of the band at about 1583 cm^{-1} (which belongs to the vibration of guanine) also decreased, revealing that the guanine conformation was altered in the presence of GNC-RGO.

In conclusion, GNCs were prepared in the organic phase by a conventional Brust–Schiffrin procedure and transferred into the aqueous phase in one step. GNCs readily interacted with RGO while keeping their size, narrow size distribution, morphology, and fluorescent properties. An MTT assay and microscopic analyses showed that GNC-RGO could cause inhibition of HepG2 cells at high concentration, but more interestingly for oncotherapy they could carry DOX inside the cells while leading to some synergy in inducing karyopyknosis. On the other hand, despite their moderate fluorescence intensity, GNC-RGO swift absorption by the cells allowed a clear imaging of the edges and morphology of the cells, thus showing interesting prospects for cellular imaging while acting as synergistic drug carriers. Finally, Raman spectroscopic investigations revealed several characteristic features substantiating the interactions between GNC-RGO nanocomposites and proteins and DNA, thus affording mechanistic clues about the origin of their inhibition of cancer cells. Generally speaking, GNC-RGO could become a multimodal probe and drug carrier for targeting, detection, and oncotherapy.

Experimental Section

Doxorubicin (DOX) was purchased from the Nanjing pharmacy factory (analytical grade). Stock solutions were freshly prepared in sterilized phosphate buffer (PBS; 0.1 M, pH 7.2) and stored in the dark at 4 °C. MTT assays were purchased from Sigma Aldrich. All the other regents used herein were analytical pure.

RGO was obtained by reduction of GO by thermal annealing to 900 °C at a heating rate of 2 °C min^{-1} and with a flow of 3% H_2/Ar stream for 12 h.[7a,b] RGO (0.8 mg) was then sonicated in chitosan aqueous solution (1.5 mL, 0.5 mg mL^{-1}) until no black sediment remained.

The dodecanethiol-modified GNCs were synthesized using a Brust–Schiffrin procedure. Typically, 6 mL of aqueous solution containing 1% m/w $HAuCl_4 \cdot 4H_2O$ was mixed with a solution of tetraoctylammonium bromide (TOAB; 169.2 mg) in chloroform (16 mL). After vigorous stirring, the $HAuCl_4$ was totally transferred into the organic phase as evidenced by a colorless aqueous layer. Dodecanethiol (40.2 μL) was then added to the organic layer with continuous stirring. A freshly prepared sodium borohydride solution (25 mL, 1.55 M) was added dropwise with further stirring for 3 h before the organic phase was recovered using a separating funnel and evaporated in a rotary evaporator (50 °C, 4 min) and resolved in chloroform (2 mL). GNCs were purified with ethanol (80 mL) through two cycles of precipitation. A chloroform–GNC solution (500 μL) containing dodecanethiol-stabilized GNCs (3.64×10^{-5} mol) was added to an aqueous solution (10 mL) of cetyltrimethylammonium bromide (CTAB; 68.56 mg) under vigorous stirring until there was no apparent phase boundary. The chloroform was then removed by quick heating to transfer GNCs into the water. The final dark-colored solution was centrifuged to remove any precipitate (Figure 1c).

The above aqueous solution of RGO was added to the aqueous solution of GNCs (3.64×10^{-5} mol) in a 10:1 molar ratio of RGO/GNCs and homogenized in an ultrasonic bath for 30 min. The above reaction mixture was incubated in the dark for 1 h to allow loading of the GNCs onto RGO. The final mixture was then separated by centrifugation at 15000 rpm for 10 min and washed with ultrapure water twice to remove the residual RGO.

A JEM-2100 transmission electron microscope (TEM) was used to characterize GNCs and GNC-RGO sizes and size distributions. Optical properties were determined with an UV/Vis-NIR absorbance spectrometer (Shimadzu, UV3600), a fluorescence spectrometer (PerkinElmer, LS-55), and a Raman spectrometer (Renishaw inVia Reflex System) according to the sought wavelength ranges.

Various concentrations of aqueous solutions of DOX were added to an aqueous dispersion of GNC-RGO nanocomposites (0.35 μg mL^{-1}) and incubated in the dark for 1 h to allow DOX loading onto the nanocomposites. Drug-loaded GNC-RGO samples were separated through centrifugation at 10000 rpm for 15 min and carefully washed three times with ultrapure water. HepG2 cells were placed in fresh cellular medium for 24 h, and then incubated with various concentrations of DOX, GNC-RGO, and DOX-loaded GNC-RGO for 48 h and 72 h accordingly. Untreated HepG2 cells were used as controls. The cell viability was measured by MTT assays.

For the cell incubation, 200 μL of HepG2 cells (ca. 5×10^5 cells mL^{-1}) were incubated with 0.25 μg mL^{-1} of GNC-RGO with or without DOX loading in cellular medium for 14 h. Cells were washed three times with PBS to remove any unbound GNC-RGO or DOX-loaded GNC-RGO accordingly before fluorescence imaging. A 490 nm excitation laser beam (Andor Revolution XD) was focused using a 20× IR coated objective (Nikon). For Raman imaging, 200 μL of HepG2 cells (ca. 5×10^5 cells mL^{-1}) were treated before and after incubation with 1.75 μg mL^{-1} GNC-RGO for 24 h. An excitation wavelength at 785 nm, 50% laser intensity, and overlaying twice with 100 s integration time was used to perform confocal Raman spectroscopy.

Received: August 6, 2011
Revised: September 5, 2011
Published online: October 11, 2011

Keywords: cancer cells · cellular interactions · drug delivery · gold nanoclusters · reduced graphene oxide

[1] a) L. A. Peyser, A. E. Vinson, A. P. Bartko, R. M. Dickson, *Science* **2001**, *291*, 103–106; b) J. Zheng, R. M. Dickson, *J. Am. Chem. Soc.* **2002**, *124*, 13982–13983; c) H. Häkkinen, S. Abbet, A. Sanchez, U. Heiz, U. Landman, *Angew. Chem.* **2003**, *115*, 1335–1338; *Angew. Chem. Int. Ed.* **2003**, *42*, 1297–1300.

[2] a) C. Gautier, T. Burgi, *J. Am. Chem. Soc.* **2008**, *130*, 7077–7084; b) C. E. Román-Velázquez, C. Noguez, I. L. Garzón, *J. Phys. Chem. B* **2003**, *107*, 12035–12038.

[3] P. Crespo, R. Litran, T. C. Rojas, M. Multigner, J. M. Fuente, J. C. Sanchez-Lopez, M. A. Garcia, A. Hernando, S. Penades, A. Fernandez, *Phys. Rev. Lett.* **2004**, *93*, 087204.

[4] a) C. L. Liu, H. T. Wu, Y. H. Hsiao, C. W. Lai, C. W. Shih, Y. K. Peng, K. C. Tang, H. W. Chang, Y. C. Chien, J. K. Hsiao, J. T. Cheng, P. T. Chou, *Angew. Chem.* **2011**, *123*, 7194–7198; *Angew. Chem. Int. Ed.* **2011**, *50*, 7056–7060; b) C. A. J. Lin, T. Y. Yang, C. H. Lee, S. H. Huang, R. A. Sperling, M. Zanella, J. K. Li, J. L. Shen, H. H. Wang, H. I. Yeh, W. J. Parak, W. H. Chang, *ACS Nano* **2009**, *3*, 395–401; c) R. Archana, S. Sonali, M. Deepthy, R. Prasanth, M. A. Habeeb Muhammed, T. Pradeep, N. Shantikumar, K. Manzoor, *Nanotechnology* **2010**, *21*, 055103; d) M. A. Habeeb Muhammed, P. K. Verma, S. K. Pal, R. C. Arun Kumar, S. Paul, R. V. Omkumar, T. Pradeep, *Chem. Eur. J.* **2009**, *15*, 10110–10120.

[5] Y. Pan, S. Neuss, A. Leifert, M. Fischler, F. Wen, U. Simon, G. Schmid, W. Brandau, W. Jahnen-Dechent, *Small* **2007**, *3*, 1941 – 1949.

[6] a) A. K. Geim, K. S. Novoselov, *Nat. Mater.* **2007**, *6*, 183 – 191; b) C. N. R. Rao, A. K. Sood, K. S. Subrahmanyam, A. Govindaraj, *Angew. Chem.* **2009**, *121*, 7890 – 7916; *Angew. Chem. Int. Ed.* **2009**, *48*, 7752 – 7777; c) S. B. Yang, X. L. Feng, L. Wang, K. Tang, J. Maier, K. Müllen, *Angew. Chem.* **2010**, *122*, 4905 – 4909; *Angew. Chem. Int. Ed.* **2010**, *49*, 4795 – 4799; d) K. P. Loh, Q. Bao, P. K. Ang, J. Yang, *J. Mater. Chem.* **2010**, *20*, 2277 – 2289; e) D. R. Dreyer, S. Park, C. W. Bielawski, R. S. Ruoff, *Chem. Soc. Rev.* **2010**, *39*, 228 – 240; f) D. R. Dreyer, R. S. Ruoff, C. W. Bielawski, *Angew. Chem.* **2010**, *122*, 9524 – 9532; *Angew. Chem. Int. Ed.* **2010**, *49*, 9336 – 9344.

[7] a) P. P. Li, Y. Chen, J. Zhu, M. Feng, X. Zhuang, Y. Lin, H. Zhan, *Chem. Eur. J.* **2011**, *17*, 780 – 785; b) C. Y. Su, Y. Xu, W. Zhang, J. Zhao, X. Tang, C. H. Tsai, L. J. Li, *Chem. Mater.* **2009**, *21*, 5674 – 5680; c) S. Stankovich, D. A. Dikin, R. D. Piner, K. A. Kohlhaas, A. Kleinhammes, Y. Jia, Y. Wu, S. T. Nguyen, R. S. Ruoff, *Carbon* **2007**, *45*, 1558 – 1565; d) H. J. Shin, K. K. Sim, A. Benayad, S. M. Yoon, H. K. Park, I. S. Jung, M. H. Jin, H. K. Jeong, J. M. Kim, J. Y. Choi, Y. H. Lee, *Adv. Funct. Mater.* **2009**, *19*, 1987 – 1992.

[8] a) T. R. Nayak, H. Andersen, V. S. Makam, C. B. S. Khaw, X. F. Xu, P. L. R. Ee, J. H. Ahn, B. H. Hong, G. Pastorin, B. Ozyilmaz, *ACS Nano* **2011**, *5*, 4670 – 4678; b) Y. K. Kim, M. H. Kim, D. H. Min, *Chem. Commun.* **2011**, *47*, 3195 – 3197; c) D. Y. Lee, Z. Khatun, J. H. Lee, Y. K. Lee, I. In, *Biomacromolecules* **2011**, *12*, 336 – 341.

[9] a) S. M. Paek, E. Yoo, I. Honma, *Nano Lett.* **2009**, *9*, 2255 – 2259; b) G. Williams, B. Seger, P. V. Kamat, *ACS Nano* **2008**, *2*, 1487 – 1491; c) J. Huang, L. M. Zhang, B. Chen, N. Ji, F. H. Chen, Y. Zhang, Z. J. Zhang, *Nanoscale* **2010**, *2*, 2733 – 2738.

[10] a) Y. Kopelevich, P. Esquinazi, *Adv. Mater.* **2007**, *19*, 4559 – 4563; b) X. Li, X. Wang, L. Zhang, S. Lee, H. Dai, *Science* **2008**, *319*, 1229 – 1232; c) S. Stankovich, D. A. Dikin, G. H. Dommett, K. M. Kohlhaas, E. J. Zimney, E. A. Stach, R. D. Piner, S. T. Nguyen, R. S. Ruoff, *Nature* **2006**, *442*, 282 – 286; d) D. A. Dikin, S. Stankovich, E. J. Zimney, R. D. Piner, G. H. Dommett, G. Evmenenko, S. T. Nguyen, R. S. Ruoff, *Nature* **2007**, *448*, 457 – 460; e) D. Li, M. B. Müller, S. Gilge, R. B. Kaner, G. G. Wallace, *Nat. Nanotechnol.* **2008**, *3*, 101 – 105; f) D. R. Dreyer, S. J. Park, C. W. Bielawski, R. S. Ruoff, *Chem. Soc. Rev.* **2010**, *39*, 228 – 240.

[11] a) S. Stankovich, R. Piner, X. Chen, N. Wu, S. T. Nguyen, R. S. Ruoff, *J. Mater. Chem.* **2006**, *16*, 155 – 158; b) Y. Xu, H. Bai, G. Lu, C. Li, G. Shi, *J. Am. Chem. Soc.* **2008**, *130*, 5856 – 5857; c) X. Yang, M. Xu, W. Qiu, X. Chen, M. Deng, J. Zhang, H. Iwai, E. Watanabe, H. Chen, *J. Mater. Chem.* **2011**, *21*, 8096 – 8103.

[12] M. Brust, M. Walker, D. Bethell, D. J. Schiffrin, R. Whyman, *J. Chem. Soc. Chem. Commun.* **1994**, *7*, 801 – 802.

[13] R. J. Zhou, M. M. Shi, X. Q. Chen, M. Wang, H. Z. Chen, *Chem. Eur. J.* **2009**, *15*, 4944 – 4951.

[14] a) O. Vrana, V. Brabee, *J. Struct. Biol.* **2007**, *159*, 1 – 8; b) J. Bandekar, S. Krimm, *Biopolymers* **1980**, *19*, 31 – 36; c) P. Crow, A. Molekovsky, N. Stone, J. B. Wilson, L. M. Wongkeesong, *Urology* **2005**, *65*, 1126 – 1130; d) G. J. J. Thomas, Y. Kyogoku, *Infrared and Raman Spectroscopy*, Biological Science, Marcel Dekker, New York, 1977, pp. 717 – 872; e) P. R. Carey, *Biochemical Applications of Raman and Resonance Raman Spectroscopies*, Academic Press, New York, **1982**, p. 71.

